

Electronic Supplementary Information

Pt single atoms meet metal–organic frameworks to enhance electrocatalytic hydrogen evolution activity

Jingting Zhu,^{a,b,c} Yingqian Cen,^b Haibin Ma,^c Weiguang Lian,^b Jidong Liu,^b Haohui Ou,^b Fangping Ouyang,^d Lifu Zhang^{a,b*} and Wenjing Zhang^{a,b*}

^a State Key Laboratory of Radio Frequency Heterogeneous Integration, Shenzhen University, Shenzhen 518060, China

^b International Collaborative Laboratory of 2D Materials for Optoelectronics Science and Technology of Ministry of Education, Institute of Microscale Optoelectronics, Shenzhen University, Shenzhen 518060, China

^c SIAMC Advanced Materials Co., Ltd., 313100, Huzhou, China

^d School of Physics and Electronics, Central South University, Changsha 410083, China.

*E-mail: wjzhang@szu.edu.cn, zhanglifu@szu.edu.cn

Table S1. The molar ratio of Pt:Fe and Pt:Cr in Pt-MIL100(Fe) and Pt-MIL101(Cr) respectively, calculated through inductively coupled plasma optical emission spectrometry (ICP-OES) measurement.

Sample	Mass fraction of Pt (wt.%)	Molar ratio (Pt:Fe)
Pt _{0.009} -MIL100(Fe)	0.55	0.009:1
Pt _{0.015} -MIL100(Fe)	0.91	0.015:1
Pt _{0.023} -MIL100(Fe)	1.41	0.023:1

Sample	Mass fraction of Pt (wt.%)	Molar ratio (Pt:Cr)
Pt _{0.011} -MIL101(Cr)	0.44	0.011:1
Pt _{0.019} -MIL101(Cr)	0.84	0.019:1
Pt _{0.034} -MIL101(Cr)	1.52	0.034:1

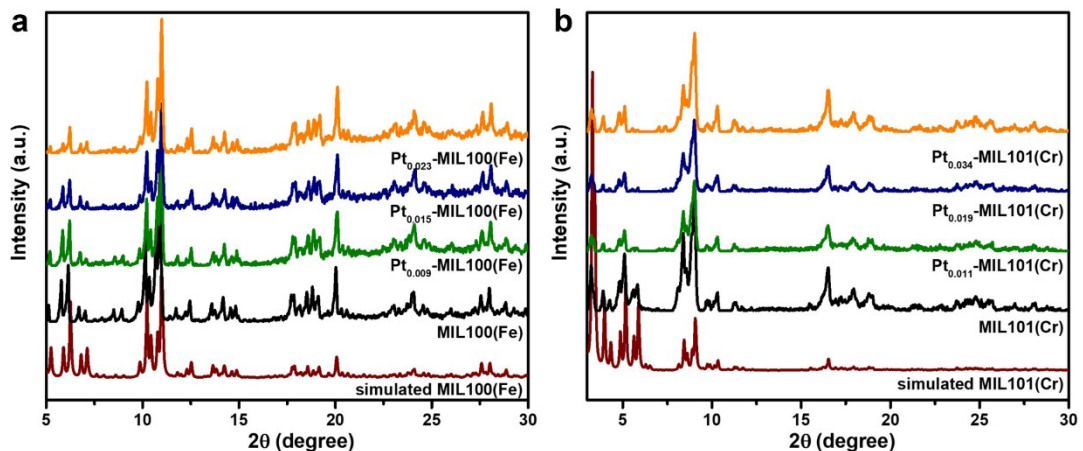


Figure S1. X-ray diffraction (XRD) patterns of **a** MIL100(Fe), Pt_{0.009}-MIL100(Fe), Pt_{0.015}-MIL100(Fe) and Pt_{0.023}-MIL100(Fe) in comparison to simulated MIL100(Fe), and **b** MIL101(Cr), Pt_{0.011}-MIL101(Cr), Pt_{0.019}-MIL101(Cr) and Pt_{0.034}-MIL101(Cr) in comparison to simulated MIL101(Cr).

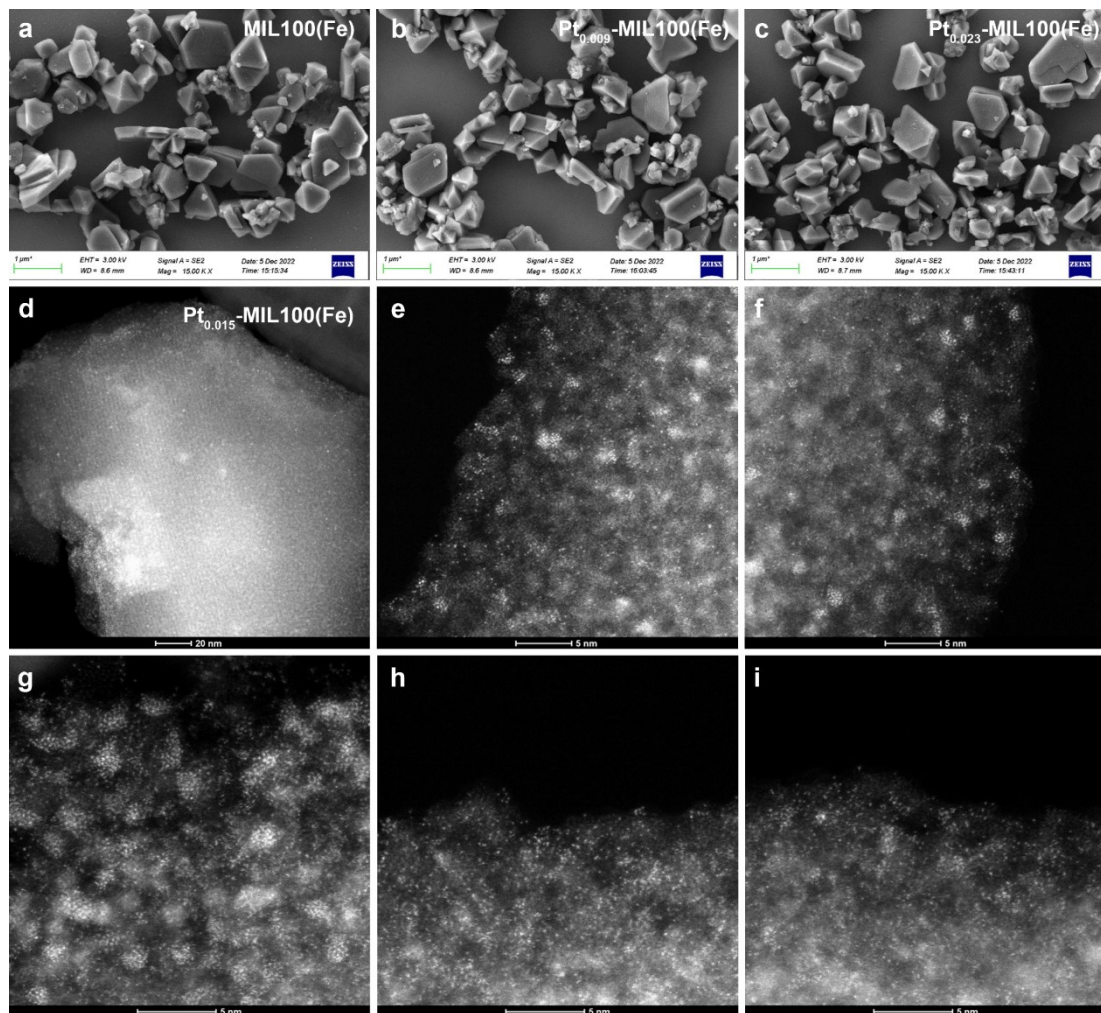


Figure S2. Scanning electron microscopy (SEM) images of **a** MIL100(Fe), **b** Pt_{0.009}-MIL100(Fe), and **c** Pt_{0.023}-MIL100(Fe). **d-i** High-angle annular dark field-scanning transmission electron microscopy (HAADF-STEM) images of Pt_{0.015}-MIL100(Fe).

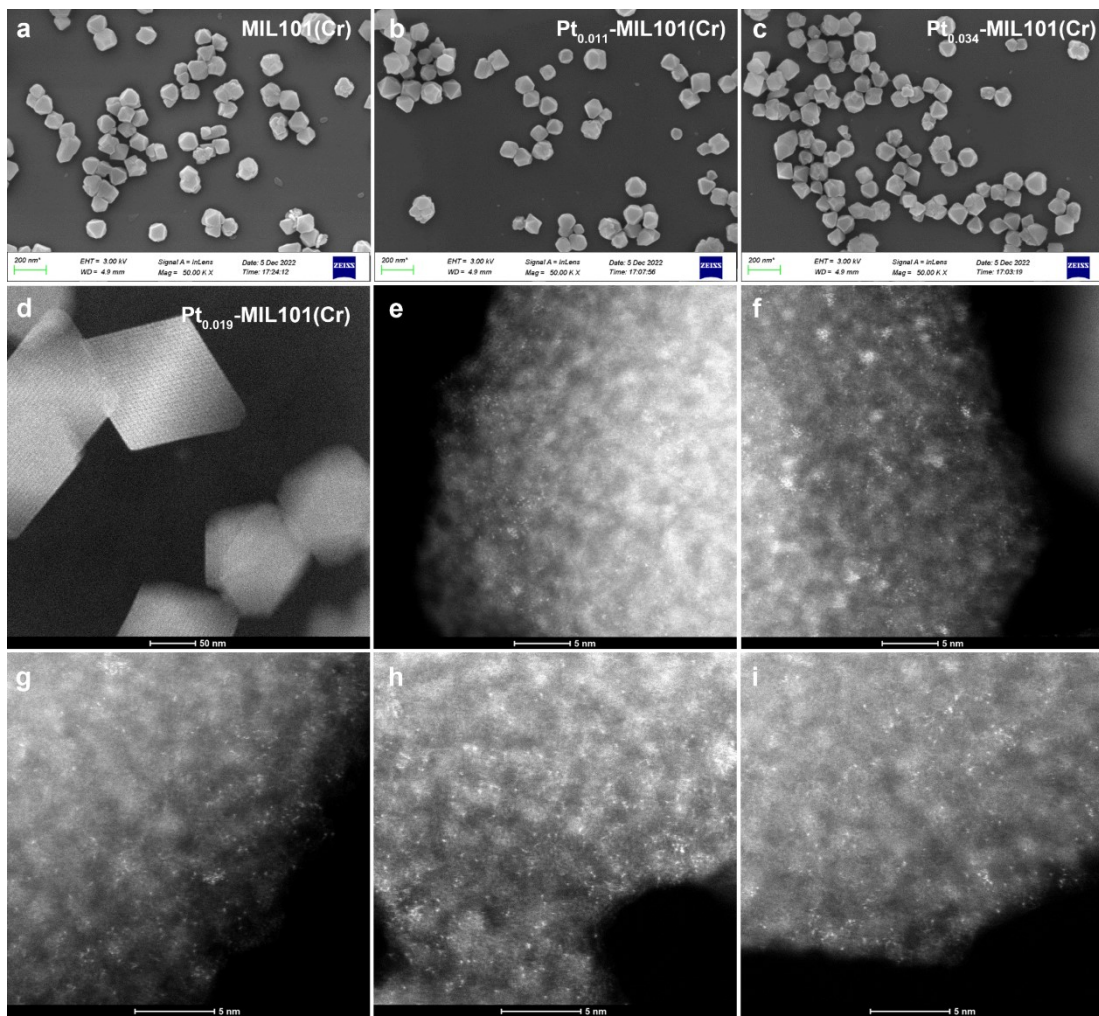


Figure S3. SEM images of **a** MIL101(Cr), **b** Pt_{0.011}-MIL101(Cr), and **c** Pt_{0.034}-MIL101(Cr). **d-i** HAADF-STEM images of Pt_{0.019}-MIL101(Cr).

Table S2. Pt L_3 -edge white-line (WL) parameters of Pt foil, Pt_{0.015}-MIL100(Fe), Pt_{0.019}-MIL101(Cr) and PtO₂.

Sample	Area (a.u.)	Oxidation state
Pt foil	1.25	0
Pt _{0.015} -MIL100(Fe)	1.58	+2.10
Pt _{0.019} -MIL101(Cr)	1.72	+2.98
PtO ₂	1.88	+4

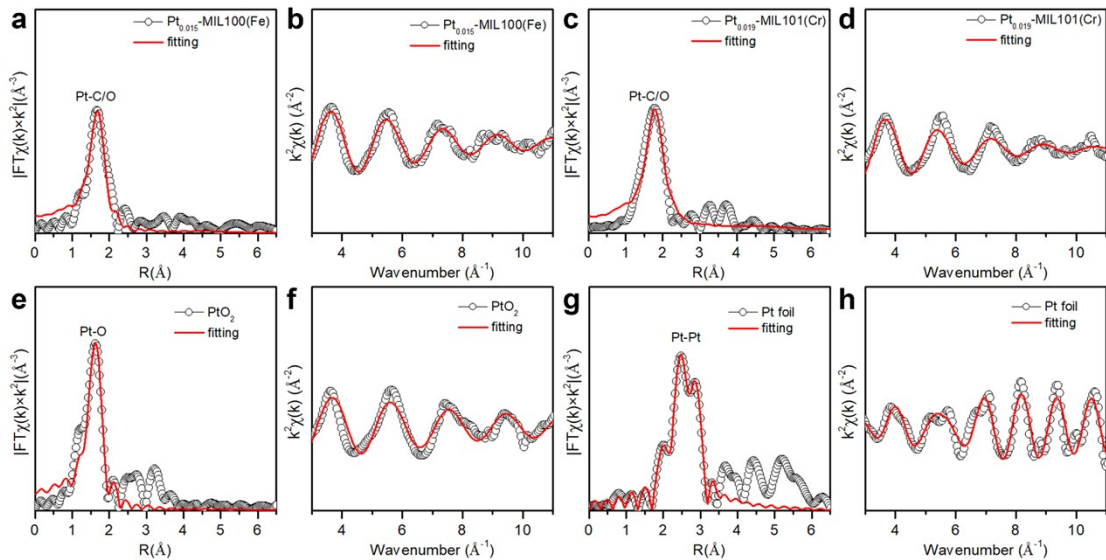


Figure S4. FT EXAFS spectra and corresponding fitting curves of the (a) $\text{Pt}_{0.015}\text{-MIL100(Fe)}$, (c) $\text{Pt}_{0.019}\text{-MIL101(Cr)}$, (e) PtO_2 and (g) Pt foil; k^2 -weighted spectra at k space of the (b) $\text{Pt}_{0.015}\text{-MIL100(Fe)}$, (d) $\text{Pt}_{0.019}\text{-MIL101(Cr)}$, (f) PtO_2 and (h) Pt foil.

Data reduction, data analysis, and EXAFS fitting were performed and analyzed with the Athena and Artemis programs of the Demeter data analysis packages¹ that utilizes the FEFF6 program² to fit the EXAFS data. The energy calibration of the sample was conducted through standard and Pt foil, which as a reference was simultaneously measured. A linear function was subtracted from the pre-edge region, then the edge jump was normalized using Athena software. The $\chi(k)$ data were isolated by subtracting a smooth, third-order polynomial approximating the absorption background of an isolated atom. The k^2 -weighted $\chi(k)$ data were Fourier transformed after applying a HanFeng window function ($\Delta k = 1.0$). For EXAFS modeling, The global amplitude EXAFS (CN , R , σ^2 and ΔE_0) were obtained by nonlinear fitting, with least-squares refinement, of the EXAFS equation to the Fourier-transformed data in R -space, using Artemis software, EXAFS of the Pt foil are fitted and the obtained amplitude reduction factor S_0^2 value (0.781) was set in the EXAFS analysis to determine the coordination numbers (CNs) in sample.

Table S3. EXAFS fitting parameters at the Pt L_3 -edge for various samples.

Sample	Shell	CN^a	$R(\text{\AA})^b$	$\sigma^2(\text{\AA}^2)^c$	$\Delta E_0(\text{eV})^d$	R factor
Pt foil	Pt-Pt	12*	2.76 ± 0.01	0.0041	7.0	0.0015
$\text{Pt}_{0.015}\text{-MIL100(Fe)}$	Pt-C/O	5.1 ± 0.3	2.07 ± 0.01	0.0035	10.5	0.0178
$\text{Pt}_{0.019}\text{-MIL101(Cr)}$	Pt-C/O	6.0 ± 0.6	2.14 ± 0.01	0.0037	10.9	0.0187
PtO_2	Pt-O	6.0 ± 0.3	2.01 ± 0.01	0.0021	11.1	0.0100

^a CN , coordination number; ^b R , distance between absorber and backscatter atoms; ^c σ^2 , Debye-Waller factor to account for both thermal and structural disorders; ^d ΔE_0 , inner potential correction; R factor indicates the goodness of the fit. S_0^2 was fixed to 0.781, according to the experimental EXAFS fit of Pt foil by fixing CN as the known crystallographic value. A reasonable range of EXAFS fitting parameters: $0.600 < S_0^2 < 1.000$; $CN > 0$; $\sigma^2 > 0 \text{ \AA}^2$; $|\Delta E_0| < 15 \text{ eV}$; R factor < 0.02 .

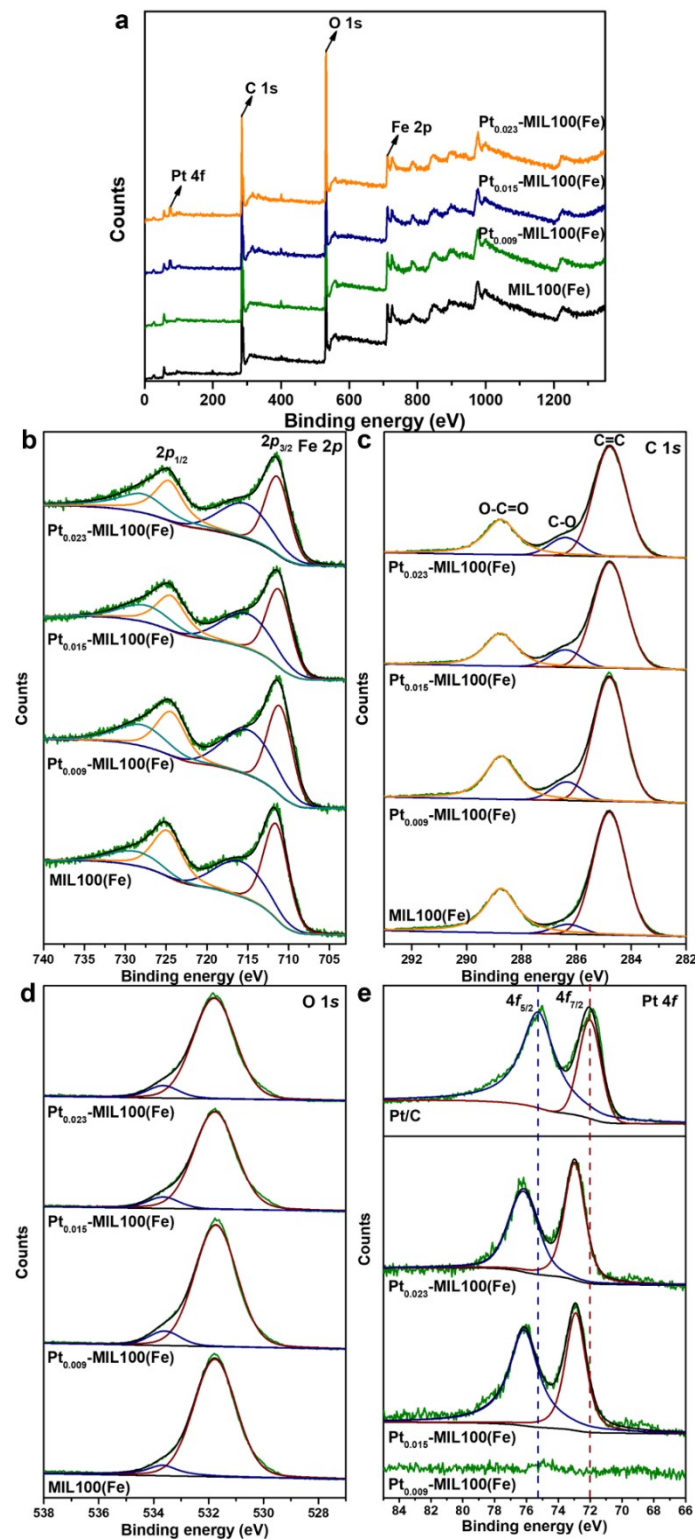


Figure S5. X-ray photoelectron spectroscopy (XPS) spectra of **a** full range, **b** Fe 2p, **c** C 1s and **d** O 1s in MIL100(Fe), Pt_{0.009}-MIL100(Fe), Pt_{0.015}-MIL100(Fe) and Pt_{0.023}-MIL100(Fe), and **e** Pt 4f in Pt_{0.009}-MIL100(Fe), Pt_{0.015}-MIL100(Fe), Pt_{0.023}-MIL100(Fe) compared to Pt/C powders.

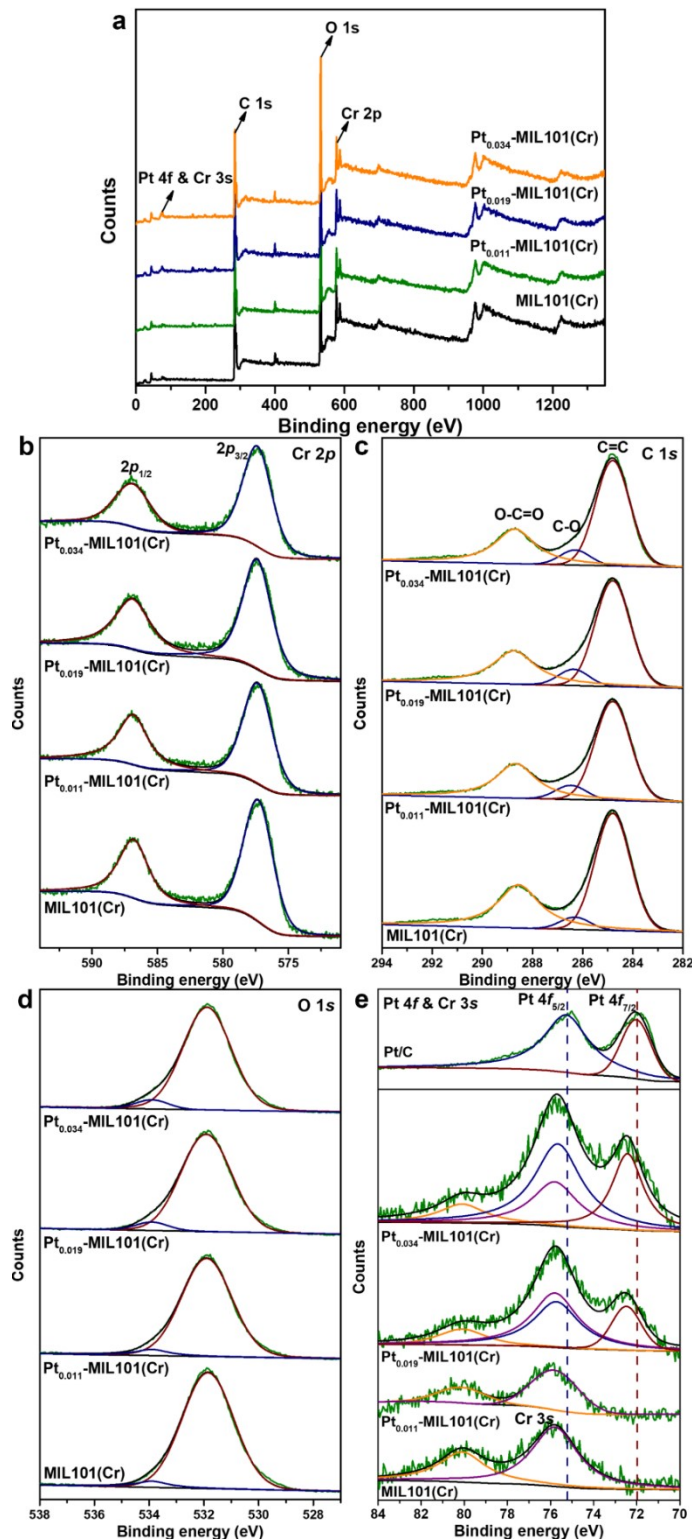


Figure S6. XPS spectra of **a** full range, **b** Cr 2p, **c** C 1s and **d** O 1s in MIL101(Cr), Pt_{0.011}-MIL101(Cr), Pt_{0.019}-MIL101(Cr) and Pt_{0.034}-MIL101(Cr), and **e** Pt 4f in Pt_{0.011}-MIL101(Cr), Pt_{0.019}-MIL101(Cr), Pt_{0.034}-MIL101(Cr) compared to Pt/C powders.

As shown in **Figure S4e**, the peaks for the normalized Pt 4f XPS spectra of Pt_{0.015-0.023}-MIL100(Fe) are visually red-shifted compared with those of metallic Pt in Pt/C. However, this result cannot be visually distinguished in Pt-MIL101(Cr) because Cr 3s peak is close to Pt 4f_{5/2} peak. When the normalized Pt 4f XPS spectra of Pt_{0.019-0.034}-MIL101(Cr) are conducted by multi-peak fitting with

the position of Cr 3s peak in MIL101(Cr) as reference, the actual positions of Pt 4f peaks marked by blue line and dark-red line can be obtained shown in **Figure S5e**. It can be seen that, consistent with Pt-MIL100(Fe) results, the Pt 4f peaks of Pt_{0.019-0.034}-MIL101(Cr) are also red-shifted compared with those of metallic Pt in Pt/C.

Table S4. HER activities of Pt SA-based catalysts in 0.5 M H₂SO₄ reported in previous literatures.

Catalyst	Content (wt.%)	Overpotential (mV) at 10 mA cm ⁻²	Tafel slope (mV/dec)	Ref.
Pt/NPC	3.8	25	28	³
Pt/NiS@Al ₂ O ₃	2.8	34	35	⁴
Pt-MXene-SWCNTs	2.8	62	78	⁵
Pt SAs/DG	2.1	23	25	⁶
Pt ₁ @Fe-N-C	2.1	60	42	⁷
Pt ₁ /MoO _{3-x}	2	23.3	28.8	⁸
Pt-PVP/TNR@GC	1.75	21	27	⁹
Pt ₁ /NMHCS	1.59	40	56	¹⁰
Pt-TiO ₂ /G	1.42	26.4	30	¹¹
Pt-SAs/C	1.26	38	43	¹²
Pt _{SA} -Mo ₂ TiC ₂ T _x	1.2	30	30	¹³
Pt-1T'MoS ₂	1.04	180	88.4	¹⁴
Pt@PCM	0.53	105	65.3	¹⁵
Pt/RuCeO _x -PA	0.49	41	31	¹⁶
Pt ₁ /OLC	0.27	38	43	¹⁷
Pt/np-Co _{0.85} Se	~1.03	55	35	¹⁸
Pt SA/WO _{3-x}	0.42	47	45	¹⁹
Pt-SA/MoS ₂	5.1	59	31	²⁰
Pt-Fe/N/C	1.5	51	48	²¹
Pt ₁ /hNCNC	2.92	15	24	²²
ALD50Pt/NGN	2.1	N.A.	29	²³
Pt ₁ /MC	2.6	N.A.	~30	²⁴
Pt ₁ /NMC	2.54	N.A.	26	²⁵
SA-Pt/MoS ₂	0.22	44	34.83	²⁶
Pt SA-VS ₂ /CP	0.65	77	40.13	²⁷
Pt-MIL100(Fe)	0.91	60	31.16	this work
Pt-MIL101(Cr)	0.84	61	27.02	this work

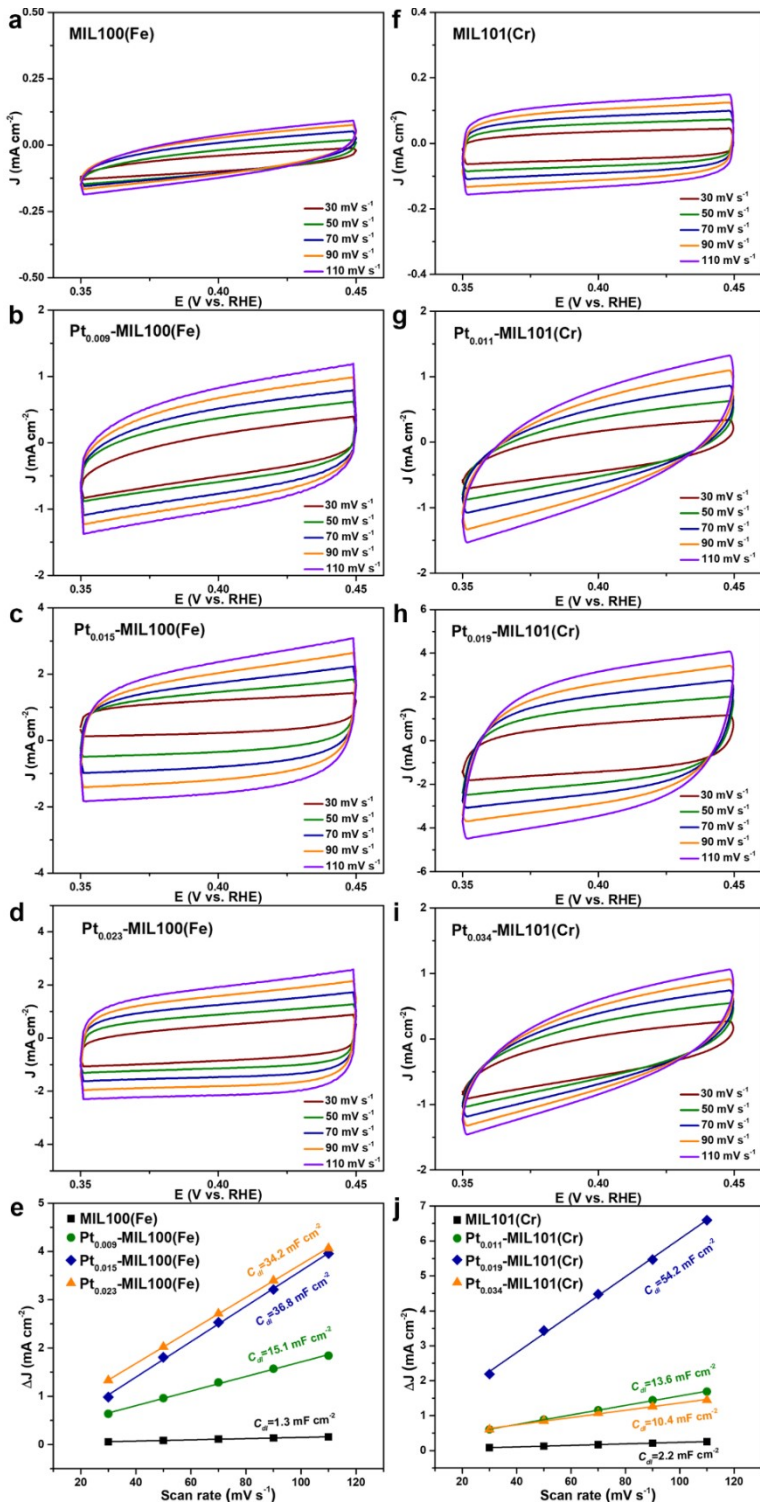


Figure S7. Cyclic Voltammograms (CV) of **a** MIL100(Fe), **b** Pt_{0.009}-MIL100(Fe), **c** Pt_{0.015}-MIL100(Fe), **d** Pt_{0.023}-MIL100(Fe), **f** MIL101(Cr), **g** Pt_{0.011}-MIL101(Cr), **h** Pt_{0.019}-MIL101(Cr), and **i** Pt_{0.034}-MIL101(Cr). Scan rate dependence of the current densities of pristine and Pt-decorated **e** MIL100(Fe) and **j** MIL101(Cr).

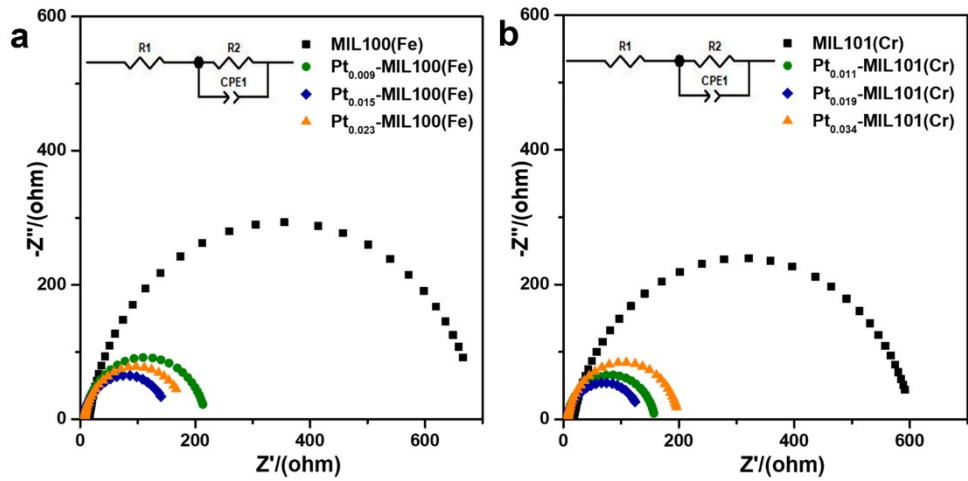


Figure S8. Nyquist plots of **a** MIL100(Fe), Pt_{0.009}-MIL100(Fe), Pt_{0.015}-MIL100(Fe) and Pt_{0.023}-MIL100(Fe), and **b** MIL101(Cr), Pt_{0.011}-MIL101(Cr), Pt_{0.019}-MIL101(Cr) and Pt_{0.034}-MIL101(Cr) tested at the overpotential of 100 mV.

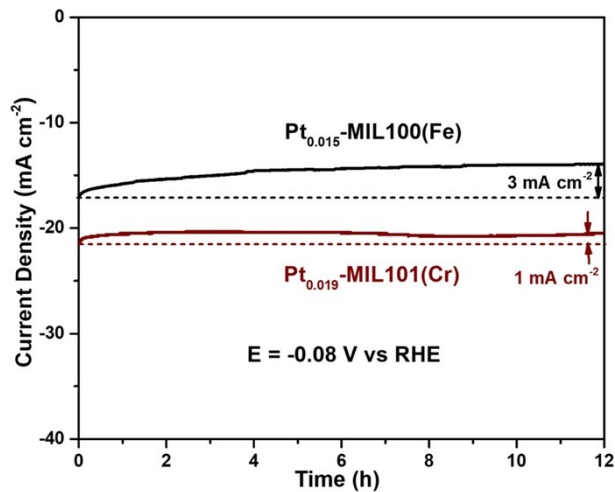


Figure S9. Time-dependent current density curve at -0.08 V vs RHE for 12h.

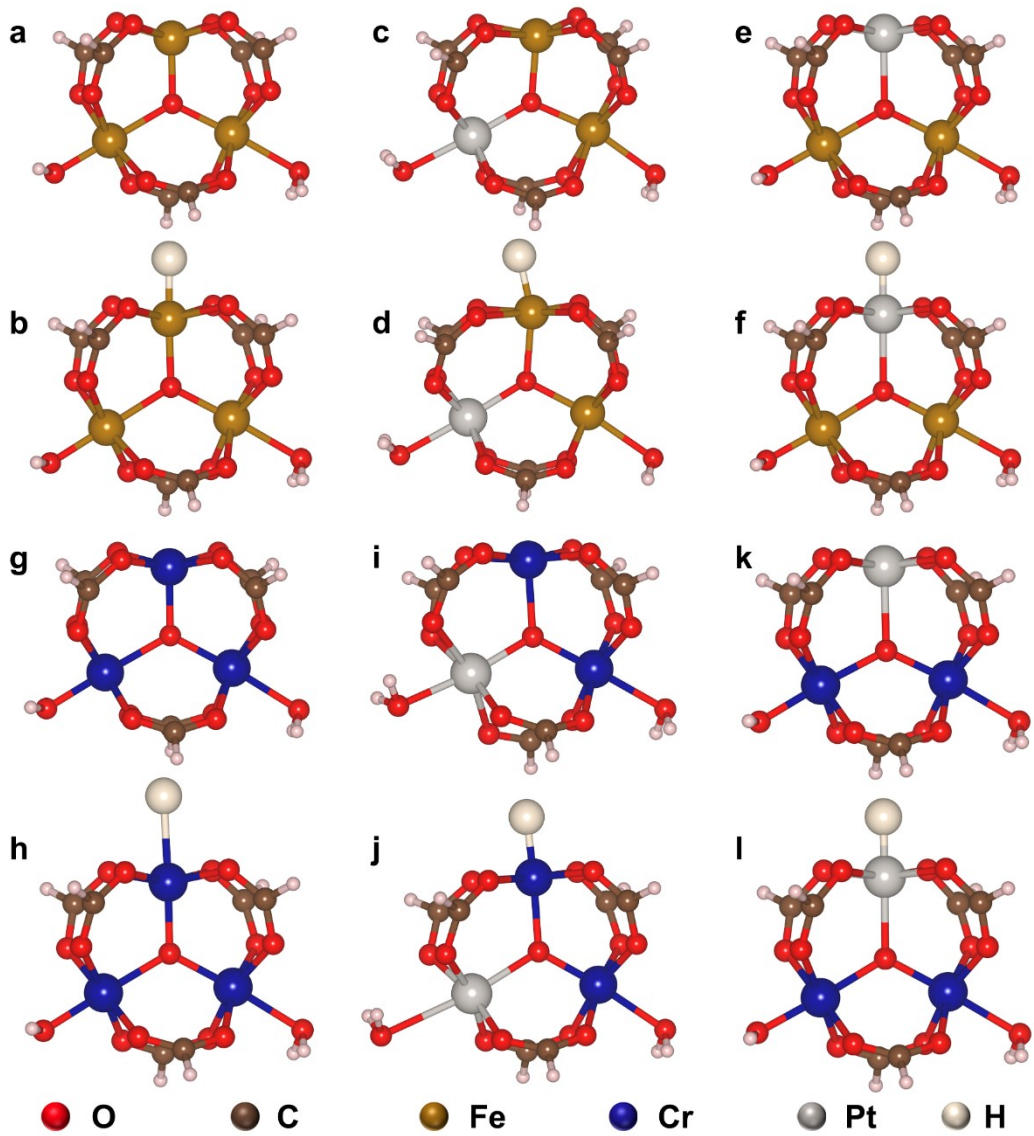


Figure S10. Optimized atomic configurations: **a** MIL100(Fe), **b** H* on Fe in **a**; **c** Pt-MIL100(Fe) (Fe atom as the active site), **d** H* on Fe in **c**; **e** Pt-MIL100(Fe) (Pt atom as the active site), **f** H* on Pt in **e**; **g** MIL101(Cr), **h** H* on Cr in **g**; **i** Pt-MIL101(Cr) (Cr atom as the active site), **j** H* on Cr in **i**; **k** Pt-MIL101(Cr) (Pt atom as the active site), **l** H* on Pt in **k**.

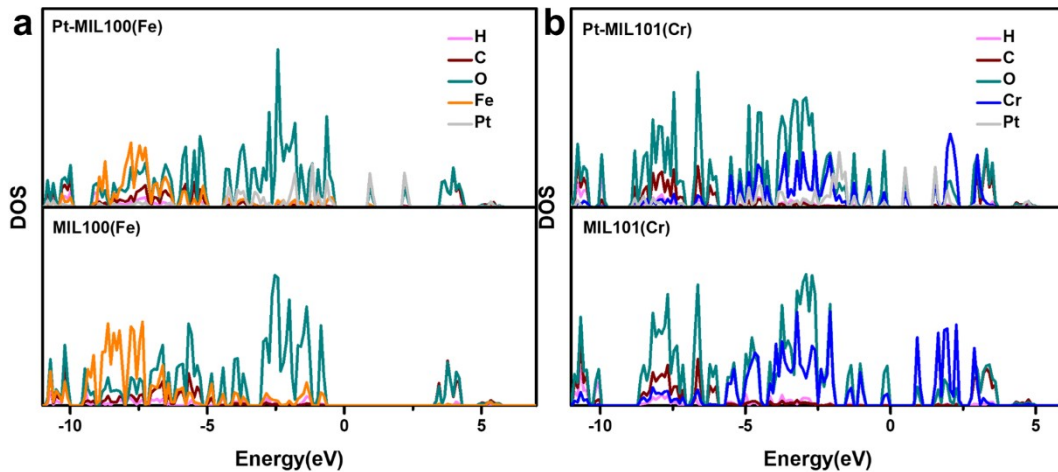


Figure S11. Calculated partial density of states (PDOS) of **a** MIL100(Fe) and Pt-MIL100(Fe), **b** MIL101(Cr) and Pt-MIL101(Cr).

Table S4. Comparison of calculated d-band centre (\mathcal{E}_d) for MIL100(Fe) and Pt-MIL100(Fe), MIL101(Cr) and Pt-MIL101(Cr) respectively.

MIL100(Fe)				
Atom ID	Fe1	Fe2	Fe3	Total
\mathcal{E}_d (eV)	-6.5313	-7.2873	-7.0869	-6.9689
Pt-MIL100(Fe)				
Atom ID	Fe1	Fe2	Pt1	Total
\mathcal{E}_d (eV)	-6.8801	-7.1461	-2.2630	-5.4835
MIL101(Cr)				
Atom ID	Cr1	Cr2	Cr3	Total
\mathcal{E}_d (eV)	-1.7644	-2.6128	-2.6732	-2.3496
Pt-MIL101(Cr)				
Atom ID	Cr1	Cr2	Pt1	Total
\mathcal{E}_d (eV)	-1.6994	-2.2984	-2.6486	-2.2106

Table S5. Calculated ΔE_{ZPE} and ΔS (unit: eV) for H^* adsorbed on the different cluster models (298.15 K).

Sample	ΔE_{ZPE}	$T\Delta S$
MIL100(Fe)	0.1391	0.0039
Pt-MIL100(Fe) (Fe atom as the active site)	0.1088	0.0057
Pt-MIL100(Fe) (Pt atom as the active site)	0.2521	0.0039
MIL101(Cr)	0.0730	0.0122
Pt-MIL101(Cr) (Cr atom as the active site)	0.1507	0.0229
Pt-MIL101(Cr) (Pt atom as the active site)	0.2480	0.0036

References

1. B. Ravel and M. Newville, *Journal of Synchrotron Radiation*, 2005, **12**, 537-541.
2. S. I. Zabinsky, J. J. Rehr, A. L. Ankudinov, R. C. Albers and M. J. Eller, *Physical Review B*, 1995, **52**, 2995-3009.
3. T. Li, J. Liu, Y. Song and F. Wang, *ACS Catalysis*, 2018, **8**, 8450-8458.
4. Y. Feng, Y. Guan, H. Zhang, Z. Huang, J. Li, Z. Jiang, X. Gu and Y. Wang, *Journal of Materials Chemistry A*, 2018, **6**, 11783-11789.
5. C. Cui, R. Cheng, H. Zhang, C. Zhang, Y. Ma, C. Shi, B. Fan, H. Wang and X. Wang, *Advanced Functional Materials*, 2020, **30**, 202000693.
6. Y. Qu, B. Chen, Z. Li, X. Duan, L. Wang, Y. Lin, T. Yuan, F. Zhou, Y. Hu, Z. Yang, C. Zhao, J. Wang, C. Zhao, Y. Hu, G. Wu, Q. Zhang, Q. Xu, B. Liu, P. Gao, R. You, W. Huang, L. Zheng, L. Gu, Y. Wu and Y. Li, *Journal of the American Chemical Society*, 2019, **141**, 4505-4509.
7. X. Zeng, J. Shui, X. Liu, Q. Liu, Y. Li, J. Shang, L. Zheng and R. Yu, *Advanced Energy Materials*, 2018, **8**, 1701345.
8. W. Liu, Q. Xu, P. Yan, J. Chen, Y. Du, S. Chu and J. Wang, *Chemcatchem*, 2018, **10**, 946-950.
9. C. Li, Z. Chen, H. Yi, Y. Cao, L. Du, Y. Hu, F. Kong, R. K. Campen, Y. Gao, C. Du, G. Yin, I. Y. Zhang and Y. Tong, *Angewandte Chemie-International Edition*, 2020, **59**, 15902-15907.
10. P. Kuang, Y. Wang, B. Zhu, F. Xia, C.-W. Tung, J. Wu, H. M. Chen and J. Yu, *Advanced Materials*, 2021, 202008599.
11. J. Ji, Z. Li, C. Hu, Y. Sha, S. Li, X. Gao, S. Zhou, T. Qiu, C. Liu, X. Su, Y. Hou, Z. Lin, S. Zhou, M. Ling and C. Liang, *ACS Applied Materials & Interfaces*, 2020, **12**, 40204-40212.
12. Z. Wang, J. Yang, J. Gan, W. Chen, F. Zhou, X. Zhou, Z. Yu, J. Zhu, X. Duan and Y. Wu, *Journal of Materials Chemistry A*, 2020, **8**, 10755-10760.
13. J. Zhang, Y. Zhao, X. Guo, C. Chen, C.-L. Dong, R.-S. Liu, C.-P. Han, Y. Li, Y. Gogotsi and G. Wang, *Nature Catalysis*, 2018, **1**, 985-992.
14. C. Wu, D. Li, S. Ding, Z. U. Rehman, Q. Liu, S. Chen, B. Zhang and L. Song, *Journal of Physical Chemistry Letters*, 2019, **10**, 6081-6087.
15. H. Zhang, P. An, W. Zhou, B. Y. Guan, P. Zhang, J. Dong and X. W. Lou, *Science Advances*, 2018, **4**, eaao6657.
16. T. Liu, W. Gao, Q. Wang, M. Dou, Z. Zhang and F. Wang, *Angewandte Chemie-International Edition*, 2020, **59**, 20423-20427.
17. D. Li, X. Li, S. Chen, H. Yang, C. Wang, C. Wu, Y. A. Haleem, S. Duan, J. Lu, B. Ge, P. M. Ajayan, Y. Luo, J. Jiang and L. Song, *Nature Energy*, 2019, **4**, 512-518.
18. K. Jiang, B. Liu, M. Luo, S. Ning, M. Peng, Y. Zhao, Y.-R. Lu, T.-S. Chan, F. M. F. de Groot and Y. Tan, *Nature Communications*, 2019, **10**, 1743.
19. J. Park, S. Lee, H.-E. Kim, A. Cho, S. Kim, Y. Ye, J. W. Han, H. Lee, J. H. Jang and J. Lee, *Angewandte Chemie International Edition*, 2019, **58**, 16038-16042.
20. Y. Shi, W. Huang, J. Li, Y. Zhou and X. Xia, *Nature Communications*, 2020, **11**, 4558.
21. H. Li, G. Wang, F. Zhang, L. Zou, Z. Zou and H. Yang, *The Journal of Physical Chemistry C*, 2020, **124**, 11760-11766.
22. Z. Zhang, Y. Chen, L. Zhou, C. Chen, Z. Han, B. Zhang, Q. Wu, L. Yang, L. Du, Y. Bu, P.

- Wang, X. Wang, H. Yang and Z. Hu, *Nature Communications*, 2019, **10**, 1657.
23. N. Cheng, S. Stambula, D. Wang, M. N. Banis, J. Liu, A. Riese, B. Xiao, R. Li, T.-K. Sham, L.-M. Liu, G. A. Botton and X. Sun, *Nature Communications*, 2016, **7**, 13638.
24. H. Wei, K. Huang, D. Wang, R. Zhang, B. Ge, J. Ma, B. Wen, S. Zhang, Q. Li, M. Lei, C. Zhang, J. Irawan, L.-M. Liu and H. Wu, *Nature Communications*, 2017, **8**, 1490.
25. H. Wei, H. Wu, K. Huang, B. Ge, J. Ma, J. Lang, D. Zu, M. Lei, Y. Yao, W. Guo and H. Wu, *Chemical Science*, 2019, **10**, 2830-2836.
26. J. Zhu, Y. Tu, L. Cai, H. Ma, Y. Chai, L. Zhang and W. Zhang, *Small*, 2022, **18**, 2104824.
27. J. Zhu, L. Cai, X. Yin, Z. Wang, L. Zhang, H. Ma, Y. Ke, Y. Du, S. Xi, A. T. S. Wee, Y. Chai and W. Zhang, *ACS Nano*, 2020, **14**, 5600-5608.